Biosensors and Bioelectronics 45 (2013) 267–273

Contents lists available at SciVerse ScienceDirect

Biosensors and Bioelectronics

journal homepage: www.elsevier.com/locate/bios

Scalable nano-bioprobes with sub-cellular resolution for cell detection

Alokik Kanwal [a], Shanmugamurthy Lakshmanan [a], Ashwini Bendiganavale [a], Corina T. Bot [a], Anitha Patlolla [b], Rahul Raj [a], Camelia Prodan [a], Zafar Iqbal [b], Gordon A. Thomas [a], Reginald C. Farrow [a,*]

[a] New Jersey Institute of Technology, Department of Physics, Newark, NJ 07102, USA
[b] New Jersey Institute of Technology, Department of Chemistry and Environmental Science, Newark, NJ 07102, USA

ARTICLE INFO

Article history:
Received 19 November 2012
Received in revised form
20 January 2013
Accepted 27 January 2013
Available online 16 February 2013

Keywords:
Cell detection
Cell identification
Bioprobes
Carbon nanotube

ABSTRACT

Here we present a carbon nanotube based device to noninvasively and quickly detect mobile single cells with the potential to maintain a high degree of spatial resolution. The device utilizes standard complementary metal oxide semiconductor (CMOS) technologies for fabrication, allowing it to be easily scalable (down to a few nanometers). Nanotubes are deposited using electrophoresis after fabrication in order to maintain CMOS compatibility. The devices are spaced by 6 μm which is the same size or smaller than a single cell. To demonstrate its capability to detect cells, we performed impedance spectroscopy on mobile human embryonic kidney (HEK) cells, neurons cells from mice, and yeast cells (*S. pombe*). Measurements were performed with and without cells and with and without nanotubes. Nanotubes were found to be crucial to successfully detect the presence of cells. The devices are also able to distinguish between cells with different characteristics.

1. Introduction

Cellular detection and identification are proving vital for the prevention and diagnosis of many diseases (Lazcka et al., 2007) related to cancer (Agarwal et al., 2007; Fang et al., 2010; Irish et al., 2004; Lin et al., 2005; Wu et al., 2003) and both viral (Caygill et al., 2010; Fang et al., 2011; Ghafar-Zadeh et al., 2009; Lien et al., 2011; Tadmor et al., 2011; Wang et al., 2011) and bacterial infections (Bhatta et al., 2010; Chalmers et al., 2007; Lu et al., 2008; Song et al., 2005; Varshney and Li, 2009; Yang and Bashir, 2008).

Techniques for cellular detection can be divided into two main categories, optical and electrical. Optical techniques rely on fluorescence of dyes attached to targeted cells. The dyes emit light when stimulated, allowing for detection through an optical microscope (Velasco-Garcia, 2009; Zhao et al., 2004). This technique has proven versatile in detecting small quantities of the targeted cells. However, the use of optical components can be expensive. In addition, the need of mixing the appropriate dyes limits the number of various types of cells that can be identified simultaneously. Also the dyes themselves can be toxic to the cells through a process called phototoxicity (Hoebe et al., 2007; Scanziani and Hausser, 2009).

Many electrical based techniques operate by measuring the change in impedance due to the presence of the target cells. These systems incorporate electrodes that measure the impedance or current between them. Currently there are two mechanisms used for electrical detection and identification of cells. The first method relies on functionalizing electrodes with a bioreceptor, which is designed to be highly selective (Caygill et al., 2010; Lu et al., 2008; Yang and Bashir, 2008). These electrodes are immersed into a solution containing the cells. The bioreceptors will bind to the targeted cell, immobilizing them on top of the electrodes. The immobilized cell will change the measured impedance or current either by insulating them or by changing the conductance of the fluid around the electrodes due to an increase in ions that surround the cells (Caygill et al., 2010; Yang and Bashir, 2008).

Microfluidic devices use a much smaller volume of cell suspension than the immersion technique. Electrodes or the walls of the fluidic channel can be functionalized to immobilize the targeted cells (Boehm et al., 2007; Cheng et al., 2007). The cell suspension is pumped through the channel and over the electrodes. The functionalized surface would capture cells as they flow over it, reducing the overall volume of suspension that is flowing between the electrodes. This will result in a change in the measured impedance or current between the electrodes.

Another electrical based technique relies on functionalizing magnetic beads with the bioreceptors instead of the electrodes or

* Corresponding author. Tel.: +1 973 596 2473.
E-mail addresses: alokik@njit.edu (A. Kanwal), sf32@njit.edu (S. Lakshmanan), ab237@njit.edu (A. Bendiganavale), ctb8@njit.edu (C.T. Bot), ap286@njit.edu (A. Patlolla), rahulraj7@gmail.com (R. Raj), cprodan@njit.edu (C. Prodan), iqbal@njit.edu (Z. Iqbal), thomasg@njit.edu (G.A. Thomas), reginald.farrow@njit.edu (R.C. Farrow).

0956-5663/$ - see front matter © 2013 Elsevier B.V. All rights reserved.
http://dx.doi.org/10.1016/j.bios.2013.01.066

walls (Yang, 2008; Varshney and Li, 2007, 2009; Yi et al., 2006). The beads are mixed with the sample, allowing the targeted cells to attach to them. After which the targeted cells are separated from the suspension by using a magnetic field. The cell-coated beads are then re-suspended in a low conductive media and either placed or flown over electrodes. The entire device is placed in a magnetic field, such that the beads are attracted to the electrode surface. The resulting accumulation of cell-coated beads lowers the impedance to indicate the presence of the targeted cells. Without the cells the drop in impedance is much smaller (Varshney and Li, 2007). This method has an advantage of having a higher sensitivity over the functionalized electrodes or walls since the magnetic beads can better cover the electrodes (Varshney and Li, 2009). However, both techniques still lack the ability to simultaneously detect a larger variety of cells in a single sample, which is required for a rapid general diagnosis.

Here we present a device that can potentially combine the benefits of optical and electrical probes using single-walled carbon nanotubes (SWNTs). Unlike optical techniques no fluorescent dyes are needed and unlike previous electrical techniques the cell does not need to be immobilized with a bioreceptor. Unlike both optical and previous electrical cell detection methods the technique reported here may provide information about the cell type and condition without modification of the cell or the probe, because we do not functionalize the nanotubes. The device can achieve high spatial resolution without significant disturbance to cells, due to the nanoscale size of the SWNTs. If the SWNT probes are made close enough, sub-cellular resolution of electrical properties down to nanometer scale could be achieved to a higher degree than both optical and previous electrical methods. Devices utilizing carbon nanotubes have been successfully fabricated to electrically detect cells or bio molecules (Balasubramanian and Burghard, 2006; Boero et al., 2012; Ishikawa et al., 2009; Li et al., 2003; Liu and Guo, 2012), however they have not yet approached the nanoscale while maintaining compatibility with semiconductor fabrication technology. Here for the first time we are reporting that an array of <10 nm diameter nanoprobes have been fabricated using a process that is fully compatible with current semiconductor technologies. The importance of this cannot be overstated, since a nanoprobe of the geometry that we are reporting would generally require either lithography that is beyond the current state of manufacturing technology or thermal cycles that are outside the requirements needed to preserve CMOS logic that will be needed to control the device. We believe that this is the main reason why such a SWNT array has never been reported. The spacing of devices in an array can scale with the current semiconductor technologies. This would allow for direct integration with the CMOS logic required for a practical lab-on-a-chip device. To demonstrate the capabilities of our device, we have used impedance spectroscopy to detect human embryonic kidney cells (HEK), yeast cells, and neuron cells harvested from mice.

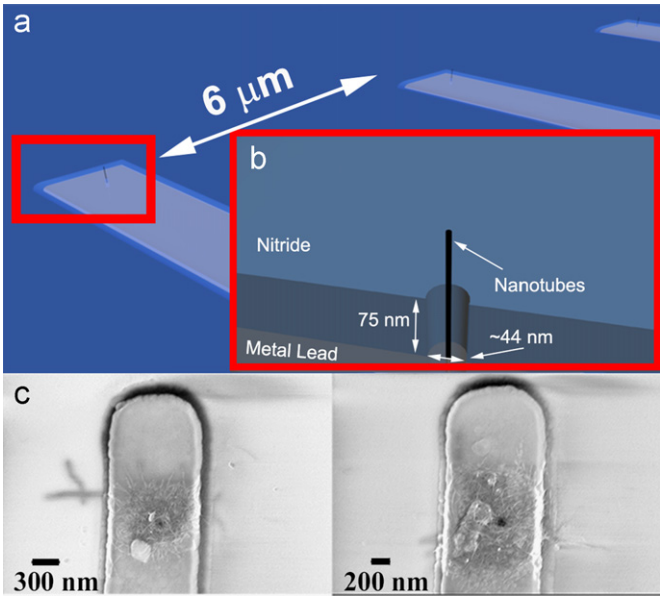

Fig. 1. (a) Schematic of a chip with multiple devices spaced 6 μm apart. (b) Zoomed in schematic of a device consisting of SWNTs connected to a metal lead through a ~44 nm window in a 75 nm thick nitride layer. (c) SEM image of nanotubes deposited into nanoscale hole at the tip of the electrodes.

2. Materials and methods

2.1. Device fabrication

2.1.1. Device substructure

Devices [shown in Fig. 1] were fabricated in a cleanroom by first depositing a 300 nm thick dielectric layer on top of clean silicon wafers. Next, a layer of photoresist was deposited and patterned using an autostepper. A metal stack consisting of 20 nm of chrome, 150 nm of cobalt, and 50 nm of chrome was subsequently evaporated without breaking vacuum. Lift off was performed to form the metal layer, consisting of six individual 1 μm wide electrodes with a 6 μm pitch. Next, 75 nm of conformal low stress silicon nitride was deposited using plasma enhanced chemical vapor deposition (PECVD). Using reactive ion etch (RIE), windows for the contact pads were opened in the nitride layer. 30–50 nm holes were then patterned using e-beam lithography. The nanoscale holes were etched using RIE, through the silicon nitride and down to the metal. The wafers were diced, producing 50 chips per wafer. Chips were subsequently glued to a chip carrier. Handling of the devices and electrical contact were thereby facilitated by wire bonding to the chip carrier's contact pads.

2.1.2. Deposition of nanotubes

Carbon nanotubes were deposited using electrophoresis [Fig. 1c], based on a method described earlier (Goyal et al., 2008). Purified SWNTs [95% metallic] were purchased from NanoIntegris. Prior to deposition, the nanotubes were horn sonicated for 6 h to reduce their lengths. During deposition, 10 V is applied between the device and a platinum rod [reference electrode], with a spacing of 1 cm between the rod and the chip. The nanotubes follow the field lines and deposit into the nanoscale holes in the nitride, and connect to the metal, forming the probes. After deposition, the devices are thoroughly rinsed to remove any stray nanotubes. Deposition of the SWNTs is verified using both SEM and Raman spectroscopy (Goyal et al., 2008).

2.2. Cell culture and harvesting

2.2.1. HEK cells

HEK cells were grown as an adherent culture in a flask. The cells were incubated at 37 °C in the presence of 5% CO_2 until they were confluent and then harvested. The growth medium used for these cells was Dulbecco's modified eagle medium (DMEM) containing 10% fetal bovine serum, penicillin streptomycin and 2 mM L-glutamine. For experiments, the flasks were treated with trypsin and incubated for 10 min. Cells were gently diluted with DMEM to annihilate the effects of trypsin and subsequently used for measurements. The conductivity of DMEM and HEK cell suspension was approximately 1.5×10^2 S/cm.

2.2.2. Yeast cells

Yeast cells were incubated in 3 ml yeast extract peptone glucose (YPD) broth in a shaker at 30 °C and 200 rpm for 48 h. The cells were then centrifuged at 1500 × *g* for 3 min. The supernatant was discarded and cells were re-suspended in 5 mM of 4-(2-hydroxyethyl)-1-piperazineethanesulfonic acid (HEPES) containing 5 mM glucose and subsequently used for measurements. Conductivity of the suspension containing HEPES buffer and yeast cells was approximately 1×10^{-4} S/cm.

2.2.3. Mouse neuron cells

Mouse neuron cells were cultured from slices of mouse brain tissue. The tissue is rinsed twice with 5 mL Hank's buffered salt solution (HBSS). Next, 5 mL of Trypsin and 0.15% of deoxyribonuclease (DNAase) is applied to the tissue and then incubated for 15–25 min at 37 °C and 5% CO_2. The tissue is then rinsed twice with 5 mL HBSS/fetal bovine serum (FBS) (4.5 mL HBSS, 0.5 mL FBS) solution, followed by rinsing twice with 5 mL HBSS only. The remaining tissue is triturated with a 1 mL pipette using DMEM. The resulting cell solution is centrifuged for 3 min at 3000 rpm. The supernatant is removed, and the cells are gently re-suspended in growth media. Next, it is filtered in a three stage process (highly porous, middle porosity, least porous). The final cell suspension is transferred to a new flask for experiments. The resulting cell media contains DMEM, similar to the HEK cells.

2.3. Experimental setup

100 μl of a suspension of cells is placed directly on top of the electrodes. The electrodes were monitored using an optical microscope. When a cell moved into position over the electrodes, a measurement was taken using a SR785 Stanford Research Systems signal analyzer and a custom built circuit (Bot and Prodan, 2009; Prodan et al., 2004) to amplify the signal. Prior to each measurement, the cells were imaged to correlate their position to the electrodes. After a set of experiments is complete, the device is thoroughly rinsed with boiling deionized water to remove any cell residue and prepare it for the next set of experiments. The resulting data was smoothed using a 10-point Savitzky–Golay method with a second order polynomial.

3. Results and discussion

Fig. 2a shows the magnitude of the impedance versus frequency for two cases, one with HEK cells and one without. The data was averaged over nine measurements. The open circles represent the presence of HEK cells over the electrodes and the squares represent the media without cells on the device. Error bars are plotted for each decade to help the legibility of the data. Fig. 2b shows an optical image of the device during a typical measurement with cells on top of the electrodes. The nanotubes are located on the ends of the electrodes, which are artificially highlighted. Noise at 60 Hz (and harmonics) was found to be present in the data, and is attributed to AC line noise, which could be reduced with refinements of the setup.

The first noticeable characteristic of the data in Fig. 2a is the increased granularity of the HEK cell measurements as compared to the relatively smooth curve that is produced without cells. In addition, the slopes appear different as highlighted by the fact that both curves start out relatively similar to each other at around 10 Hz but diverge significantly at higher frequencies, particularly above 10 kHz. The unique morphology of the HEK cell curve might be indicative of cell motility. The cells were not fixed to the surface, and were free to move around. We used this property to avoid using a micromanipulator to position the cells. As such, during each measurement the cells can move slightly and even vibrate. The velocities of the cells were measured by analyzing the distance they moved per measurement. Cells on the devices moved slower than those away from the devices. On the device, cells moved on average about 0.6 μm per minute. The cells away from the device ranged from 0.6 to 12 μm per minute. Those that moved quickly are believed to be above the surface. Based on the focal plane, the slower cells, including those on the devices, are believed to be in contact with the surface which retards their motion. Other cell characteristics, such as ion channel kinetics or membrane reactions to the nanotubes might also be related to granularity of the curve, however further experiments are needed to understand the source of granularity and its significance. The sharp differences in impedance with and without cells suggest that an impedance measurement between closely spaced nanoprobes is capable of detecting the presence of the HEK cells.

To demonstrate the versatility of our device, we used different types of cells. In addition to the HEK cells, we looked at neuron cells from mice and yeast cells. High-resolution images of the three types of cells are shown in Fig. 3(a)–(c). One big difference in the cells is their size and shape. The HEK cells are round and average in size between 16 and 30 μm, while the yeast cells range from 6 to 10 μm. In contrast, neurons have a more amorphous shape and range in size from 18 to 28 μm. Both the HEK and neuron cells are larger than the probe spacing [6 μm], while the

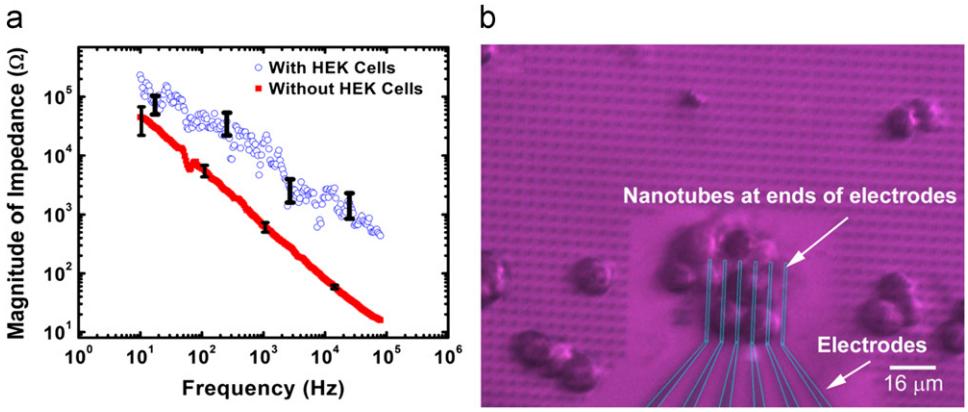

Fig. 2. (a) Magnitude of the impedance vs. frequency for two cases. The open circles represent HEK cells on top of the electrodes and the squares represent the case without cells. Error bars are plotted for each decade. (b) Optical image during a measurement of HEK cells. The actual interconnect metal and nanoprobes in the image are underneath the cells. The location of the interconnects (labeled electrodes in the image) were ascertained from the CAD file used during device fabrication and added to the original image for clarity.

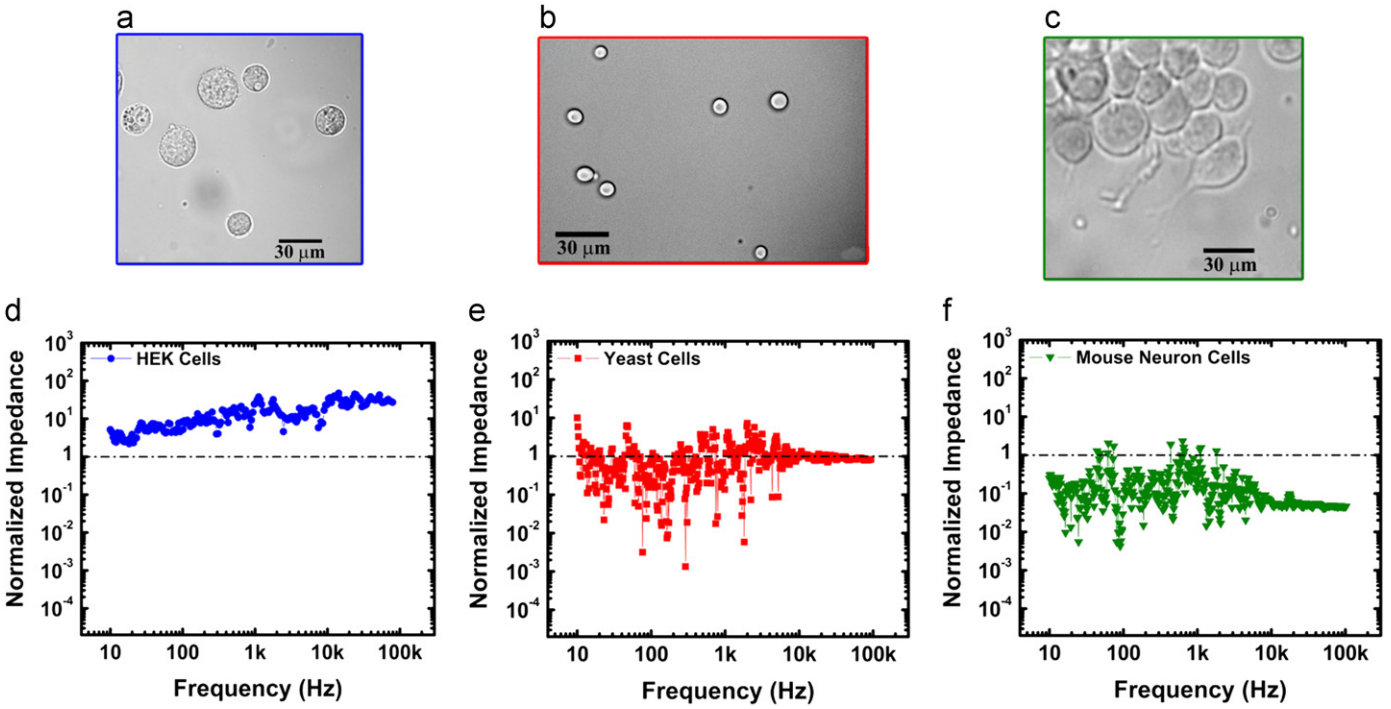

Fig. 3. High resolution images of (a) HEK cells, (b) yeast cells and (c) mouse neuron cells. Normalized impedance of (d) HEK cells, (e) yeast cells and (f) mouse neuron cells.

yeast cells are similar or larger. The difference between cell size and probe spacing allows for a single cell measurement with a small degree of sub-cellular resolution for the three cell types. The resulting impedance spectra of the cells were normalized by dividing out their case without cells on the electrodes. The normalized impedance spectra are shown in Fig. 3(d)–(f). A value of 1 is an indication that the measurements with and without cells are similar and can be thought of as a baseline. The dotted line represents this baseline. The data without cells, which makes up the baseline, did not appear to be significantly affected by measurements with cells [see supplementary material].

The different cell types appear to have distinct properties in their impedance spectra. The HEK spectrum starts out at 8 around 10 Hz but then increase to around 25 at high frequencies. This is in stark contrast to both the yeast cells and the neuron cells, which tend to trend less than one. For the yeast cells the affect is less pronounced and only at low frequencies. Neuron cells overall experience a drop in impedance when a cell is over the electrodes. This seems unexpected since adding a dielectric material in between the electrodes should raise the impedance. The drop could be attributed to the neurons themselves. It could be possible that the neuron cells were interacting with the carbon nanotubes. Neuron cells have been known to respond to electrical stimuli from electrodes including nanotubes (Mazzatenta et al., 2007; Polikov et al., 2005). If the nanotube electrodes could stimulate the neuron cells, they could respond by releasing a range of ions which change the conductivity of the media around the cells and thus between the nanoprobes. However, more work will need to be done to better understand this.

Both the yeast and the neuron cells impedance traces have structure to their curves. Interestingly though, the granularity of the curves appears to be more than that of the HEK cells. This could be attributed to the fact that the HEK cells are model cells, designed to study ion channels (Cockerill et al., 2007; Ducroq et al., 2007; Zhou et al., 1998). As such, the ions around the HEK cells are limited to potassium and sodium ions (Zhou et al., 1998) which are used to maintain osmotic pressure across the membrane and to maintain a membrane potential, thus creating less variation in the extracellular material surrounding the cells as compared to the yeast and neuron cells. The extra types of ions surrounding the yeast cells include organic acid from metabolizing sugar and oxygen (Yang and Bashir, 2008), while the neuron cell contain additional ions such as Ca^{2+} and amino acids used by the cells for communications (Cowan et al., 2001). The three different extracellular environments could create unique structures in the impedance spectra for the three types of cells.

Another possible explanation of the difference in the spectra for each type of cell is cell motility. The neuron cell's velocities ranged from 0.9 to 16 μm per minute, where the higher velocity cells were above the surface. This is similar to the HEK cells which ranged from 0.6 to 12 μm per minute. The yeast cell's velocity could not be measured due to the complete cell coverage of the field of view, which prevented identification of any one cell for tracking. While the cell motility could play a role in the impedance spectra, the data does not seem to support it. The neuron cells are the largest and the yeast cells are the smallest, while the HEK cells are in the middle in terms of size. It is reasonable to consider the cell motility to be dominated by Brownian motion, which is dependent on size. This effect does correlate with the neuron cell's velocity being slightly larger than the HEK cells. If the variation in the impedance spectra were dependent on motility then the measured impedance spectras would deviate from their respective baseline, either as increasing or decreasing impedance, with the amount of deviation being related to the size of the cell. However, this does not seem to be the case. Instead the largest (neuron cells) and the smallest (yeast cells) both experience a drop in impedance while the middle sized cells (HEK cell) experience a rise in impedance. While it is conceivable that cell motility can play a role in the impedance spectra, its influence could be a secondary effect and not a primary one.

To summarize, there are many cell characteristics that may have contributed to the differences in the normalized impedance shown in Fig. 3. Some of these characteristics may or may not be associated with cell type. That is, the data is too preliminary to

attribute a specific signature in the impedance to cell type. More controlled experiments are needed and possibly other measurement modes to establish a direct association of the data with cell type.

In order to better understand the roles the nanotubes play, impedance measurements were repeated using devices where nanotube were not deposited. Fig. 4(a) shows an SEM image of the devices, which consists of a pair of 1 μm wide electrodes with ~44 nm windows in the silicon nitride layer, leading down to the metal. During nanotube deposition, the nanotubes would deposit within these windows. Without the nanotubes, the metal at the base of the nanosized windows generate the electric field used in the impedance measurements as opposed to the sharp tip of the nanotube.

The resulting impedance spectra for HEK cells, neuron cells, and yeast cells are shown in Fig. 4(b)–(d) respectively. The most striking feature is the lack of shift on average between measurements taken with and without cells. This is in stark contrast to those taken with nanotubes. With nanotubes as probes, there was significant increase in impedance with HEK cells and a significant drop with neuron and yeast cells. The nanotubes obviously play an important role in the impedance measurements of the various cell types, and may even be interacting with the cells. Three other possibilities could be occurring as well. The first is that without the nanotubes, the 75 nm deep holes (aspect ratio of 2:1 [depth:-diameter]) could be deep enough to reduce the sensitivity of the devices as compared to the nanotube devices. Planar geometry microscale probes can detect single cells using impedance spectroscopy when the cells are in close proximity (i.e. in direct contact) (Jiang and Spencer, 2010). In our case the window geometry is needed to control the deposition of the SWNTs, which precludes direct contact with the cells to our probes unless there are SWNTs. The geometry of the SWNTs may also increase the sensitivity of the impedance measurement. The relative sharp tips of the nanotubes (~1 nm) are known to have electric field enhancements (Wang et al., 1997; Zhong et al., 2002). This focuses and increases the field strength at the nanotubes tips, thus allowing the measurement to be more sensitive than ~44 nm planar electrodes. Another possibility is in the difference in materials. Without nanotubes, Cr (used as the metal at the bottom of the windows) is the electrode surface. Metals such as Cr may not be as good as carbon (which is relatively inert and biocompatible) for electrodes used in bio experiments, potentially due to oxidation and other possible electrochemical effects. This could reduce the sensitivity as compared to the nanotube measurements. Further research is required to better understand these potential effects.

Based on the results from the devices with and without nanotubes, we can speak to the type of measurement occurring. Comparing the two types of devices, the electric field between the 1 μm wide electrodes is going to be the same between the nanotube and nanoscale window devices. The differences occur locally at the location of the ~44 nm windows and the nanotubes, due to the radical differences in geometry. The field enhancement from the nanotubes will concentrate the field lines closer together, thus increasing its strength as compared to the relatively flat electrode surface at the bottom of the ~44 nm window. This effect is similar to the tip enhancements in atomic force microscopy surface-enhanced Raman spectroscopy (AFM-SERS) of particles, where the sharp tips enhance and focus the electric fields to a small part of the particle (Micic et al., 2003). This could give a strong interaction with the mobile charges in and around the cell creating relatively large polarization effects that may be responsible for the changes in impedance. It must be pointed out that the interface between the CNTs and the metal interconnects has not been characterized for this deposition method. Even though CNTs can form low resistance contacts with metals such as Cr, Ti, and Fe (Lim et al., 2009), it does not

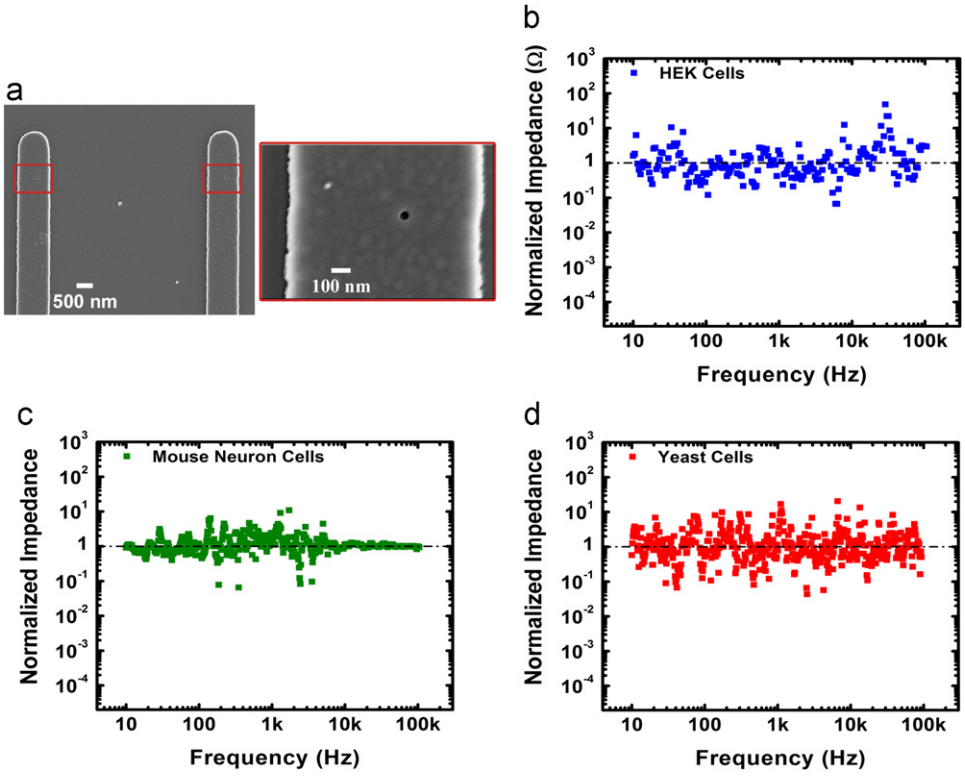

Fig. 4. (a) SEM image of electrodes without nanotubes. Inset is a zoomed image from an area within one of the rectangles of a ~44 nm window used for measurements. Impedance magnitude spectrum for devices without nanotubes for (b) HEK cell, (c) mouse neuron cells, and (d) yeast cells.

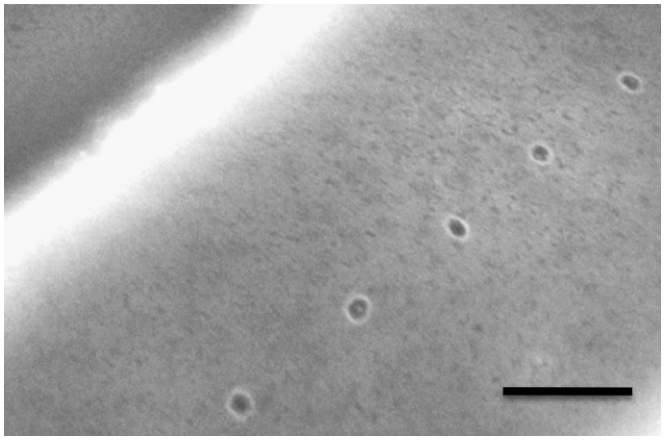

Fig. 5. SEM image of SWNTs deposited using electrophoresis on Ti at the base of 30–40 nm windows (75 nm deep) spaced 200 nm apart. The scale bar is 200 nm.

necessarily follow that after electrophoresis deposition the contacts are ohmic. Further experiments and modeling are required to see how the CNT/metal contact affects the device. However, the current device structure does enable one to detect and distinguish between the cell types that were measured. Keeping these factors in mind, it is conceivable that the measurement from the nanotubes is occurring on the two parts of the cell membrane which are closest to the two nanotube probes, as opposed to a whole cell measurement. If a whole cell measurement was occurring, then the nanoscale window devices would be able to detect the presence of cells, albeit perhaps not at the same sensitivity as the nanotubes devices, but this does not seem to be the case.

One of the key advances in this study is the demonstration of a sub-10 nm probe using the current generation of CMOS process technology (including lithography). This is made possible by the novel deposition technology reported by Goyal et al. (2008). It uses electrophoresis in conjunction with nanoscopic lenses to deposit the SWNTs in a controlled fashion. Since the deposition is done at room temperature, it does not suffer the deleterious effects normally imposed by growing SWNTs using chemical vapor deposition (CVD) at relatively high temperatures ($>300\ ^{\circ}C$) (Ren et al., 1998) or the need to control the diameter of the SWNT using lithography that cannot be used in the current generation of manufacturing technology (Duesberg et al., 2004; Graham et al., 2004). The limit to the spacing between SWCNTs is set by current CMOS process technology, which is established by the International Technology Roadmap for Semiconductors (ITRS) (Semiconductor Industry Association, 2011). Windows in thin dielectrics that are 30–40 nm in diameter are readily available in the current generation for DRAM contact windows. When the limits to level-to-level overlay are taken into account, the practical limitation using current CMOS process technology is $\sim$50 nm wide interconnect lines with 50 nm spacing, which leads to center-to-center window spacing of $\sim$100 nm. The current generation of window sizes does not appear to limit the electrophoresis deposition as indicated in Fig. 5. In this case SWNTs that were presorted to be <180 nm long (Fagan et al., 2008) were deposited on Ti metal at the base of 30–40 nm windows (75 nm deep) spaced 200 nm apart.

4. Conclusions

We have successfully fabricated devices for detecting cells using vertically deposited carbon nanotubes. The devices are planar and have small enough inter-nanotube spacing to allow for single cell measurements using pairs of probes. Our use of standard CMOS technologies and self-alignment allows for scaling of future devices down to the nanometer scale. Our method can reduce complexity and cost compared to other technologies. In addition, multiple devices of the same kind could be arranged in a high-density array, allowing for simultaneous measurements across a single cell or a group of cells. Experiments are currently underway to understand the device's performance at the nanoscale and within arrays.

Our current device successfully performed impedance measurements on HEK cells. Measurements with and without cells showed a significant difference, indicating that we can detect the cells. We also measured neurons from mice and yeast cells, which exhibited different spectra from those of HEK cells. This difference in the spectrum indicates that the devices could distinguish between different cell characteristics. In addition, since we did not rely on actively positioning or impaling the cells, we were able to make the measurements without significantly disturbing them.

We also carried out measurements on devices without nanotubes on the three cell types. The resulting spectra showed no average shift between data with and without cells. The similarity indicates that the nanotubes play a crucial role in electrically probing the cells, and could interact with the cells directly. In addition, the device could probe small sections of the cell membrane.

The unique spectrums of impedance as a function of frequency for the three different cell types hints at the possibility that the device could be used to study electrostatics and dynamics of various cells. Given enough research, devices of this type may have the potential to be used in experiments to look at action potentials, study ion channels, membrane potentials, and subcellular processes, with a high degree of spatial resolution (nanometer range) without disturbing the cells or requiring the cells to be immobilized.

Acknowledgments

The authors would like to thank DARPA for funding the research (FA9550-05-1-0461, FA8650-08-1-7825 and N00014-08-1-0278) and Cornell Nanofabrication Facility (CNF) and its staff for the use of their cleanroom and expert advice during fabrication. The authors would also like to thank Prof. Andrew Hill and Kyle Dobiszewski for their help with the mice neurons, Dr. Jeffrey Fagan of the National Institute of Standards and Technology for providing the carbon nanotubes sorted by length, and Dr. Heiner Jaksch of Carl Zeiss for performing the high resolution SEM of the nanotubes deposited in the 200 nm spaced windows.

Appendix A. Supporting information

Supplementary data associated with this article can be found in the online version at http://dx.doi.org/10.1016/j.bios.2013.01.066.

References

Agarwal, A., Huang, S.W., O'Donnell, M., Day, K.C., Day, M., Kotov, N., Ashkenazi, S., 2007. Journal of Applied Physics 102 (6), 064701–064704.
Balasubramanian, K., Burghard, M., 2006. Analytical and Bioanalytical Chemistry 385 (3), 452–468.
Bhatta, D., Stadden, E., Hashem, E., Sparrow, I.J.G., Emmerson, G.D., 2010. Sensors and Actuators B: Chemical 149 (1), 233–238.
Boehm, D.A., Gottlieb, P.A., Hua, S.Z., 2007. Sensors and Actuators B: Chemical 126 (2), 508–514.
Boero, C., Olivo, J., Micheli, G.D., Carrara, S., 2012. IEEE Transactions on Biomedical Circuits and Systems 6 (5), 479–485.
Bot, C., Prodan, C., 2009. European Biophysics Journal 38 (8), 1049–1059.
Caygill, R.L., Blair, G.E., Millner, P.A., 2010. Analytica Chimica Acta 681 (1-2), 8–15.

Chalmers, N.I., Palmer, R.J.J., Du-Thumm, L., Sullivan, R., Shi, W., Kolenbrander, P.E., 2007. Applied and Environmental Microbiology 73 (2), 630–636.
Cheng, X., Liu, Y.-s., Irimia, D., Demirci, U., Yang, L., Zamir, L., Rodriguez, W.R., Toner, M., Bashir, R., 2007. Lab on a Chip 7 (6), 746–755.
Cockerill, S.L., Tobin, A.B., Torrecilla, I., Willars, G.B., Standen, N.B., Mitcheson, J.S., 2007. The Journal of Physiology 581 (2), 479–493.
Cowan, W.M., Südhof, T.C., Stevens, C.F., 2001. Synapses. The Johns Hopkins University Press, Baltimore.
Ducroq, J., Printemps, R., Guilbot, S., Gardette, J., Salvetat, C., Grand, M.L., 2007. Journal of Pharmacological and Toxicological Methods 56 (2), 159–170.
Duesberg, S.G., Graham, P.A., Kreupl, F., Liebau, M., Seidel, R., Unger, E., Hoenlein, W., 2004. Diamond and Related Materials 13 (2), 354–361.
Fagan, A.J., Becker, L.M., Chun, J., Hobbie, K.E., 2008. Advanced Materials 20 (9), 1609–1613.
Fang, C., Wang, Y., Vu, N.T., Lin, W.-Y., Hsieh, Y.-T., Rubbi, L., Phelps, M.E., Müschen, M., Kim, Y.-M., Chatziioannou, A.F., Tseng, H.-R., Graeber, T.G., 2010. Cancer Research 70 (21), 8299–8308.
Fang, Y., Ye, P., Wang, X., Xu, X., Reisen, W., 2011. Journal of Virological Methods 173 (2), 251–258.
Ghafar-Zadeh, E., Sawan, M., Therriault, D., 2009. IEEE Transactions on Advanced Packaging 32 (2), 410–416.
Goyal, A., Liu, S., Iqbal, Z., Fetter, L.A., Farrow, R.C., 2008. Journal of Vacuum Science and Technology B 26, 2524–2528.
Graham, P.A., Duesberg, S.G., Seidel, R., Liebau, M., Unger, E., Kreupl, F., Hönlein, W., 2004. Diamond and Related Materials 13 (4–8), 1296–1300.
Hoebe, R.A., Oven, C.H.V., Gadella, T.W.J., Dhonukshe, P.B., Noorden, C.J.F.V., Manders, E.M.M., 2007. Nature Biotechnology 25 (2), 249–253.
Irish, J.M., Hovland, R., Krutzik, P.O., Perez, O.D., Bruserud, Ø., Gjertsen, B.T., Nolan, G.P., 2004. Cell 118 (2), 217–228.
Ishikawa, N.F., Stauffer, B., Caron, A.D., Zhou, C., 2009. Biosensors and Bioelectronics 24 (10), 2967–2972.
Jiang, X., Spencer, M.G., 2010. Biosensors and Bioelectronics 25 (7), 1622–1628.
Lazcka, O., Campo, F.J.D., Muñoz, F.X., 2007. Biosensors and Bioelectronics 22 (7), 1205–1217.
Li, J., Ng, H.T., Cassell, A., Fan, W., Chen, H., Ye, Q., Koehne, J., Han, J., Meyyappan, M., 2003. Nano Letters 3 (5), 597–602.
Lien, K.-Y., Hung, L.-Y., Huang, T.-B., Tsai, Y.-C., Lei, H.-Y., Lee, G.-B., 2011. Biosensors and Bioelectronics 26 (9), 3900–3907.
Lim, S.C., Jang, J.H., Bae, D.J., Han, G.H., Lee, S., Yeo, I.-S., Lee, Y.H., 2009. Applied Physics Letters 95 (26), 264103–264105.
Lin, A.W.H., Lewinski, N.A., West, J.L., Halas, N.J., Drezek, R.A., 2005. Journal of Biomedical Optics 10 (6), 064035.
Liu, S., Guo, X., 2012. NPG Asia Materials 4, e23.
Lu, Y.-C., Chuang, Y.-S., Chen, Y.-Y., Shu, A.-C., Hsu, H.-Y., Chang, H.-Y., Yew, T.-R., 2008. Biosensors and Bioelectronics 23 (12), 1856–1861.
Mazzatenta, A., Giugliano, M., Campidelli, S., Gambazzi, L., Businaro, L., Markram, H., Prato, M., Ballerini, L., 2007. Journal of Neuroscience 27 (26), 6931–6936.
Micic, M., Klymyshyn, N., Suh, Y.D., Lu, H.P., 2003. The Journal of Physical Chemistry B 107 (7), 1574–1584.
Polikov, V.S., Tresco, P.A., Reichert, W.M., 2005. Journal of Neuroscience Methods 148 (1), 1–18.
Prodan, C., Mayo, F., Claycomb, J.R., Miller, J.H., Benedik, M.J., 2004. Journal of Applied Physics 95, 3754–3756.
Ren, F.Z., Huang, P.Z., Xu, W.J., Wang, H.J., Bush, P., Siegal, P.M., Provencio, N.P., 1998. Science 282, 1105–1107.
Semiconductor Industry Association, 2011. International Technology Roadmap for Semiconductors. 〈http://www.itrs.net/Links/2011ITRS/Home2011.htm〉.
Scanziani, M., Hausser, M., 2009. Nature 461 (7266), 930–939.
Song, J.M., Culha, M., Kasili, P.M., Griffin, G.D., Vo-Dinh, T., 2005. Biosensors and Bioelectronics 20 (11), 2203–2209.
Tadmor, A.D., Ottesen, E.A., Leadbetter, J.R., Phillips, R., 2011. Science 333 (6038), 58–62.
Varshney, M., Li, Y., 2007. Biosensors and Bioelectronics 22 (11), 2408–2414.
Varshney, M., Li, Y., 2009. Biosensors and Bioelectronics 24 (10), 2951–2960.
Velasco-Garcia, M.N., 2009. Seminars in Cell and Developmental Biology 20 (1), 27–33.
Wang, Q.H., Corrigan, T.D., Dai, J.Y., Chang, R.P.H., Krauss, A.R., 1997. Applied Physics Letters 70 (24), 3308–3310.
Wang, R., Lin, J., Lassiter, K., Srinivasan, B., Lin, L., Lu, H., Tung, S., Hargis, B., Bottje, W., Berghman, L., Li, Y., 2011. Journal of Virological Methods 178 (1–2), 52–58.
Wu, X., Liu, H., Liu, J., Haley, K.N., Treadway, J.A., Larson, J.P., Ge, N., Peale, F., Bruchez, M.P., 2003. Nature Biotechnology 21 (1), 41–46.
Yang, L., 2008. Talanta 74 (5), 1621–1629.
Yang, L., Bashir, R., 2008. Biotechnology Advances 26 (2), 135–150.
Yi, C., Li, C.-W., Ji, S., Yang, M., 2006. Analytica Chimica Acta 560 (1–2), 1–23.
Zhao, X., Hilliard, L.R., Mechery, S.J., Wang, Y., Bagwe, R.P., Jin, S., Tan, W., 2004. Proceedings of the National Academy of Sciences of the United States of America 101 (42), 15027–15032.
Zhong, D.Y., Zhang, G.Y., Liu, S., Sakurai, T., Wang, E.G., 2002. Applied Physics Letters 80 (3), 506–508.
Zhou, Z., Gong, Q., Ye, B., Fan, Z., Makielski, C.J., Robertson, A.G., January, T.C., 1998. Biophysical Journal 74 (1), 230–241.